ARL-TR-9605 ● Oct 2022

DEVCOM ARMY RESEARCH LABORATORY

# Characterizing Entangled Photon Source Performance as a Function of Temperature

by Atiyya A Davis, Thomas A Searles, Brian T Kirby, and Daniel E Jones

## NOTICES

### Disclaimers

The findings in this report are not to be construed as an official Department of the Army position unless so designated by other authorized documents.

Citation of manufacturer's or trade names does not constitute an official endorsement or approval of the use thereof.

Destroy this report when it is no longer needed. Do not return it to the originator.

ARL-TR-9605 ● OCT 2022


# Characterizing Entangled Photon Source Performance as a Function of Temperature

**Atiyya A Davis and Thomas A Searles**
*University of Illinois Chicago*

**Brian T Kirby and Daniel E Jones**
*DEVCOM Army Research Laboratory*

# REPORT DOCUMENTATION PAGE

*Form Approved*
*OMB No. 0704-0188*



| 1. REPORT DATE *(DD-MM-YYYY)* | 2. REPORT TYPE | 3. DATES COVERED (From - To) |
|---|---|---|
| October 2022 | Technical Report | 1 March–30 September 2022 |

**4. TITLE AND SUBTITLE**
Characterizing Entangled Photon Source Performance as a Function of Temperature

**5a. CONTRACT NUMBER**

**5b. GRANT NUMBER**

**5c. PROGRAM ELEMENT NUMBER**

**6. AUTHOR(S)**
Atiyya A Davis, Thomas A Searles, Brian T Kirby, and Daniel E Jones

**5d. PROJECT NUMBER**

**5e. TASK NUMBER**

**5f. WORK UNIT NUMBER**

**7. PERFORMING ORGANIZATION NAME(S) AND ADDRESS(ES)**
DEVCOM Army Research Laboratory
ATTN: FCDD-RLC-NT
Adelphi, MD 20783

**8. PERFORMING ORGANIZATION REPORT NUMBER**
ARL-TR-9605

**9. SPONSORING/MONITORING AGENCY NAME(S) AND ADDRESS(ES)**

**10. SPONSOR/MONITOR'S ACRONYM(S)**

**11. SPONSOR/MONITOR'S REPORT NUMBER(S)**

**12. DISTRIBUTION/AVAILABILITY STATEMENT**
Approved for public release: distribution unlimited.

**13. SUPPLEMENTARY NOTES**
ORCID IDs: Atiyya A Davis: 0000-0002-0184-9095; Thomas A Searles: 0000-0002-0532-7884; Brian T Kirby: 0000-0002-2698-9887; Daniel E Jones: 0000-0002-9854-5767

**14. ABSTRACT**
Quantum network users require knowledge of their entangled photon source performance, the types of noise photons that are output by their source, and the regimes that their sources must be operated in to maximize entanglement quality. Here, we describe a method to characterize the behavior of an entangled photon source as a function of temperature, power, and frequency. We provide an analysis of the entangled photon source performance by performing quantum state tomography and by measuring the coincidence to accidental ratio. We find that noise photons due to Raman scattering and spectral broadening of the pump caused by self-phase modulation significantly reduce the performance of the source in certain operating regimes. In addition, we determine what temperature, power, and output channels should be used to maximize the entanglement quality of the source.

**15. SUBJECT TERMS**
quantum networks, quantum communication, entanglement, entangled photon sources, Network and Computational Sciences, Photonics, Electronics, and Quantum Sciences

| 16. SECURITY CLASSIFICATION OF: | | | 17. LIMITATION OF ABSTRACT | 18. NUMBER OF PAGES | 19a. NAME OF RESPONSIBLE PERSON |
|---|---|---|---|---|---|
| a. REPORT | b. ABSTRACT | c. THIS PAGE | | | Daniel Jones |
| Unclassified | Unclassified | Unclassified | UU | 21 | 19b. TELEPHONE NUMBER (Include area code) 301-394-0503 |

## Contents

## List of Figures

# 1. Introduction

Quantum networks offer possible performance benefits over their classical counterparts for various communication and computing applications. However, these fundamental quantum networking primitives will require significant technological advances in several areas of basic research. Regardless of the eventual use case, quantum networks must be able to store, manipulate, distribute, and generate quantum states. The latter requirement of generating quantum states is generally performed with an entangled photon source (EPS). Ideally, an EPS would create on-demand noiseless entangled photons. In practice, however, EPSs are probabilistic and can be impacted by multiple forms of noise, many due to nonlinear optical effects within the EPS itself. Therefore, effectively realizing a quantum network will require intimate knowledge of what types of noise are present in various operating regimes of the EPS and how to mitigate the effects of those types of noise.

Entangled photon sources based on four-wave mixing (FWM) in the zero-dispersion region of optical fibers[1,2] are a common type of EPS that are even available commercially.[3] These sources can be easily integrated into existing fiber networks with very low loss due to the benefit of the entangled photons being inherently fiber-based. However, these sources output additional noise photons due to Raman-scattering and self-phase modulation (SPM) of the pump laser, so steps must be taken to characterize the amount of these photons that are output in various regimes to maximize the performance of the source.

In this report we describe a method to characterize the behavior of the NuCrypt entangled photon distribution system located in the US Army Combat Capabilities Development Command Army Research Laboratory Quantum Network Testbed as a function of temperature, power, and frequency. First we describe the experimental setup, which consists of a NuCrypt EPS, two polarization analyzers (PAs), and a correlated photon detection system (CPDS). We then explain how the EPS was characterized by performing quantum state tomography, by analyzing the concurrence of the quantum state output by the EPS, and by measuring the coincidence-to-accidental ratio (CAR) of light output by the EPS. Finally, we analyze the concurrence and CAR data to determine the optimum operating parameters of the EPS.

# 2. Experimental Setup

## 2.1 Description of NuCrypt Entangled Photon Source

The experimental setup consists of a NuCrypt EPS, two PAs, and a CPDS. A schematic diagram of our experiment to characterize the EPS is shown in Fig. 1. The EPS generates signal and idler photons via FWM by pumping a dispersion shifted fiber (DSF) with a 50-MHz pulsed fiber laser at 1552.52 nm (International Telecommunication Union [ITU] Channel 31). The DSF is arranged in a Sagnac loop with a polarizing beam splitter (PBS) to entangle the signal and idler photons in polarization, creating a $|\varphi^+\rangle$ Bell state.[4] The FWM process results in signal and idler photons with a broadband spectrum, but the EPS demultiplexes them into Channels 26–29 (1556.56–1554.13 nm) and 33–36 (1550.92–1548.51 nm) on the 100-GHz-spaced ITU grid.

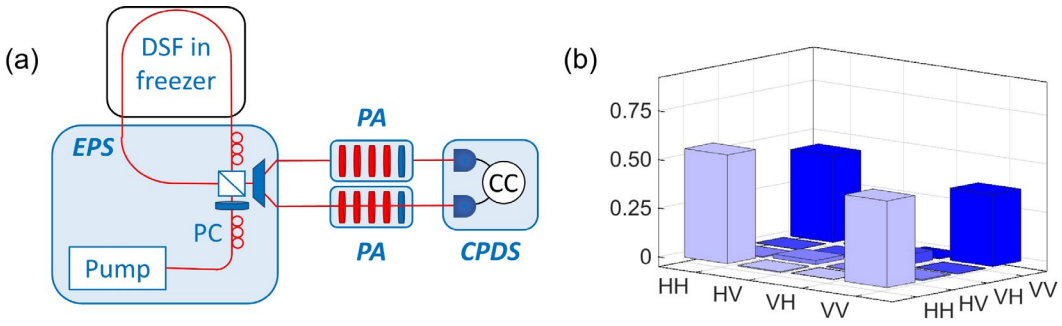


**Fig. 1 (a) Schematic diagram of the experimental setup. The PAs are kept in place when performing quantum state tomography (see Section 3.1) but removed when performing CAR measurements (see Section 3.2). Notes: PC = polarization controller; CC = coincidence-counting electronics. (b) Real part of an example density matrix measured by tomography.**

The PAs include various waveplates and a polarizer in order to perform a measurement at any angle on the Bloch sphere, and the CPDS includes two indium gallium arsenide (InGaAs) single-photon detectors (~20% detection efficiency; dark count probability $\sim 4 \times 10^{-5}$ per gate) and the electronics necessary to perform coincidence measurements between the two detectors. Detailed instructions for operating the NuCrypt EPS, PAs, and CPDS are included in Jones et al.[5]

## 2.2 Types of Photons Output by the Source

The EPS generates time–energy entangled photon pairs through FWM, a $\chi(3)$ nonlinear optical process. Since two photons are necessarily created at the same time from two pump photons, the output photons exhibit frequency (energy) correlations due to conservation of energy. As stated in the previous section, the

signal and idler photons are then entangled in polarization by placing the DSF in a Sagnac loop with a PBS. In addition to FWM, the EPS also generates photons due to SPM[6,7] and Raman scattering.[8–11] Previously we have characterized the effects of various sources of noise and channel imperfections in optical fiber channels,[12–16] but here we investigate the effect of noise photons created by the EPS itself due to SPM and Raman scattering.

SPM is also a $\chi(3)$ nonlinear optical process and results in a spectral broadening of the pump laser, which can cause leakage of additional noise photons into the output channels of the EPS (i.e., into Channels 26–29 and 33–36). We can predict that SPM photons would predominantly affect the inner-most channel pair (29/33), as they are most susceptible to pump leakage due to their small detuning from the pump (Channel 31). On the other hand, Raman-scattering results from the nonlinear interaction of pump photons with phonons and also causes additional noise photons to be generated in the EPS output channels. Contrary to SPM, Raman scattering increases as the detuning from the pump laser increases, so channel pair 26/36 is expected to have the greatest amount of Raman-scattered noise photons. The ability to reduce the number of Raman-scattered photons by cooling the DSF has been well-documented.[17–24] For further details on quantifying the amount of Raman photons output by our source at room temperature, see Jones et al.[25,26]

## 2.3 Procedure to Operate NuCrypt System

To begin characterizing the EPS, the EPS, PAs, and CPDS must be connected by single-mode optical fibers. Before connecting each device, the fiber end faces must be cleaned and examined using an optical fiber microscope to ensure there are no defects or scratches on the fiber tip. Once the fiber tips have been properly cleaned, they are connected to the output channels of the EPS. Since the two photons of a FWM pair are symmetric about the pump frequency (Channel 31) due to conservation of energy, the appropriate correlated channel pairs must be used (i.e., Channels 26/36, 27/35, 28/34, and 29/33) to detect photons of the same FWM pair. If the appropriate output channels are not connected, fewer coincidences will be measured since uncorrelated photons are being detected.

Once the EPS, PAs, and CPDS are properly connected by fibers, each must be connected to the laboratory computer by USB and powered on to prepare for use. Next, run the NuCrypt Entangled Photon Analyzer (EPA) software on the laboratory computer. After opening the software, press “identify” to display what devices are connected to the computer by USB. Panels for the EPS, PAs, and CPDS are displayed, and the connected devices are shown in each corresponding panel. In the CPDS control panel, unassign Slots 3 and 4 since the CPDS used here only

has two detectors. In the PA panel, set the wavelength for each channel in use (i.e., 1556.56 nm for Channel 26, 1555.75 nm for Channel 27, 1554.94 nm for Channel 28, 1554.13 nm for Channel 29, 1550.92 nm for Channel 33, 1550.12 nm for Channel 34, 1549.32 nm for Channel 35, and 1548.52 nm for Channel 36). Next click "eps init" to adjust the pump polarization to 45°. To produce a maximally entangled state, the pump must be set at 45° at the input of the Sagnac loop's PBS. During the initialization, the internal PC is automatically adjusted until the power at the output of the Sagnac loop is maximized, signifying that the pump is set to 45°. The front display panel on the EPS will display the maximum power value (in microwatts [μW]) after initializing. If the setup and initialization are successful, the front panel value should read greater than 340 μW when the EPA "light" setting (which sets the pump power) is 3600. Note that this benchmark value is subject to change due to various factors such as changes to the DSF and connections between the various ports and fibers of the EPS. Users should make note of the benchmark value corresponding to proper initialization of the pump for their EPS/setup.

On the CPDS panel, set the number of gates to 50 million, then proceed by clicking "CPDS ctrl" to open a new window that allows for greater control of the CPDS settings. This window includes a "Configuration" panel to set the bias and threshold for each detector of the CPDS and a "Synchronization" panel to set the relative delay of the two detectors to ensure that photons from the same pair are detected at the same time. The bias and threshold for each detector must then be adjusted. First, click the gate phase button on Channel 1 to scan the gate phase for Detector 1. A pop-up window will appear displaying the number of counts during the gate phase scan. The EPA software then automatically sets the detector phase to the setting at which the maximum counts were measured, thus properly locating the arrival time of the photons. If additional peaks or other nonphysical features appear, the detector bias and threshold must be entirely reset. Refer to Jones et al.[5] for details on how to reset the detector bias and threshold for optimum performance. After adjusting the detector settings, click "measure" under the dark count panel on the original EPA screen. A warning message will be displayed if the dark count rate is too high. Continue adjusting the bias and/or threshold as needed until an ideal dark count rate ($\sim 4 \times 10^{-5}$ per gate; varies for each detector) is achieved. Next, repeat these steps for Detector 2.

Now the relative delay of Detectors 1 and 2 must be set in order to measure coincidences between photons generated by the EPS in Channels 1 and 2 at the same time. In the synchronization section, select "c12" and "d1." This delays Detector 1 by an integer number of pump pulses (20 ns) and measures the number of coincidences between Detectors 1 and 2. The EPA software then scans the Detector 1 delay over the user-entered range and sets the delay to the value that

maximizes the number of coincidences. For the CPDS used here, Channel 2 is electronically delayed relative to Channel 1, so Channel 1 must be delayed in the EPA software to detect a pair of photons at Detectors 1 and 2 at the same time. Enter "0" in the box labeled "start" and "12" in the box labeled "end." This adjusts the delay of Channel 1 over 12 different values and measures the coincidences of Detectors 1 and 2 for each delay. Note that the magnitude of the delay will change if significantly different lengths of fiber are used in Channels 1 and 2. The NuCrypt system is now ready for operation.

## 3. Characterizing EPS Performance

In this section we describe the methods for performing quantum state tomography and CAR measurements to characterize the performance of the EPS and determine the optimum operating parameters for minimizing the effects of Raman scattering and SPM. Quantum state tomography[27] is the process by which the density matrix, which completely describes the quantum state of a system, is determined by measuring the output of that system many times. For a source of two-photon polarization-entangled states like our EPS, this can be accomplished by measuring the coincident detections of both photons in 36 different joint polarization bases. Note that the 36 measurement settings used in our experiment are not unique and that other configurations are possible, either through the use of additional detectors or by choosing different measurement bases. However, regardless of the configuration of our tomographic setup, any complete reconstruction should result in an identical outcome.

CAR measurements, on the other hand, do not directly determine the quantum state of a system but provide valuable information about the relative number of entangled photons to noise photons output by an EPS. CAR is the ratio of the measured coincidences divided by the expected number of accidental coincidences of two detectors, where an accidental coincidence is defined as the event in which two uncorrelated photons are simultaneously detected by two detectors by chance. This statistically occurs with a probability given by the product of the probabilities that each detector detects one of the uncorrelated single photons during a given time.

### 3.1 Perform Quantum State Tomography to Measure Entanglement

To perform tomography, start by adjusting the freezer that holds the DSF to the desired temperature. For this report, the temperature ranges from +20 to –86 °C (the minimum operating temperature of our freezer). Using the EPA software, adjust the light setting to the desired value (3100–3800) to adjust the

power of the pump laser using an attenuator inside of the EPS. The pump power is measured at the output of the Sagnac loop and is displayed on the EPS front panel. Record the power displayed on the EPS for each light setting entered in the EPA software. Next enter the number of detection gates (measurement time). The number of gates should be set such that the maximum number of coincidences measured for any of the 36 tomography bases is greater than 1000. On the tomography panel, check the "max likelihood" and "stack" boxes. The "max likelihood" setting results in a maximum likelihood estimation (MLE)[28] being performed to determine the density matrix from the tomography measurements. Unchecking the box results in a linear fit to the tomography measurements. This typically is faster but less accurate than MLE. Additional quantum state estimation techniques based on machine learning[29–32] and Bayesian estimation[33,34] are also currently being investigated as replacements for MLE-based tomography. The "stack" option causes the EPA software to automatically output a plot of the density matrix upon completion of each tomography run.

Next, set the number of runs to the desired amount (here we use 10), then click "start." The EPA software automatically controls the CPDS and PAs to perform full polarization state tomography by performing measurements in 36 different joint polarization bases. The number of coincident detections between Detectors 1 and 2 for the set number of detection gates is recorded for all 36 bases, and the MLE of the density matrix is performed for each run. The tomography results, including the density matrix, maximum coincidences, and various entanglement metrics, are recorded in a separate window for each run. The raw detector measurements (single counts for each detector, coincident detections, and accidental detections) are saved in a text file titled "tomoXXX," where XXX represents the number assigned to the dataset and increases automatically when tomography is complete. The calculated density matrix and corresponding entanglement metrics are saved in the text file titled "tomoXXX_Analysis." Repeat this process for the remaining power settings. After performing tomography 10 times for each power setting, repeat the process for all remaining correlated channel pairs (as described in Section 2.3) at the same temperature. Finally, repeat all of the steps for each temperature.

The average concurrence for each of the 10 runs per experimental setting (temperature, power, and channel pair) is then calculated. Concurrence is an entanglement metric that varies from 0 to 1, with 0 corresponding to a separable state with no entanglement and 1 corresponding to a maximally entangled state. The concurrence is shown for each channel pair as a function of attenuation at +20 and –86 °C in Fig. 2(a) and (b), respectively. All attenuation values are calculated relative to the maximum power (i.e., for an EPA light setting of 3800). Specifically, the attenuation was calculated by $attn = 10\log_{10}(P/P_{max})$, where $P$ is the pump

power displayed on the EPS front panel for a given data point and $P_{max}$ is the power displayed on the EPS front panel for a light setting of 3800. The error bars are calculated from the standard deviation of the concurrence for each of the 10 runs.

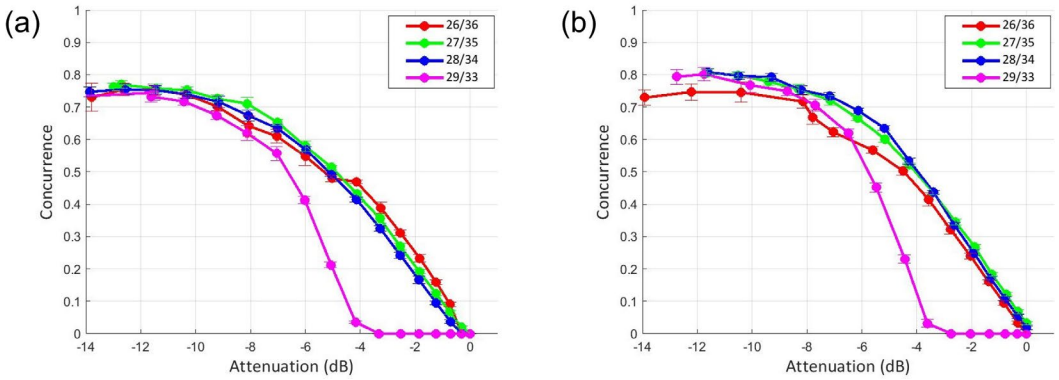


**Fig. 2 Concurrence as a function of pump attenuation when the DSF is stored at (a) +20 °C and (b) –86 °C. The decrease in concurrence is seemingly due to spectral broadening of the pump caused by SPM. This decrease in concurrence is greatest for the inner-most channel pair (29/33) since that channel pair has the smallest detuning from the pump (Channel 31).**

As described in Section 2.2, our EPS outputs entangled photons created by FWM, noise photons due to Raman scattering, and noise photons due to SPM-induced broadening of the pump. FWM photon pairs scale quadratically in power; Raman-scattered photons scale linearly in power; and SPM scales quadratically in power. Since both FWM photons of a pair are necessarily created at the same time, coincidences due to FWM photons also scale quadratically. However, noise photons (both Raman-scattered and SPM) are created independently, so coincidences due to noise photons scale as the product of the individual probabilities of generating a noise photon in each channel. Therefore, coincidences due to Raman-scattering scale quadratically in power, but coincidences due to SPM scale as $\sim P^4$. Due to the different power dependence of entangled and noise photons, as power increases (attenuation decreases), the relative number of accidental coincidences due to SPM increases and concurrence decreases. This effect is particularly noticeable in Channels 29/33, the channels that are least detuned from the pump channel (31) since these channels are most susceptible to leakage of SPM-broadened pump photons. See Ma et al.[6] and Morosova et al.[7] for more details on the statistics of photons created by FWM, Raman scattering, and SPM.

The concurrence is shown for each channel pair as a function of DSF temperature with a pump attenuation of approximately 12.5 dB in Fig. 3. Once again, the error bars are calculated from the standard deviation of the concurrence for each of the 10 runs at that power and temperature. The average concurrence for all channel

pairs increases from 0.74 to 0.79 as the temperature of the DSF is decreased from +20 to –86 °C due to a reduction in Raman-scattered photons. This is in agreement with previous reports[17–24] of reducing the number of Raman-scattered photons by cooling the DSF.

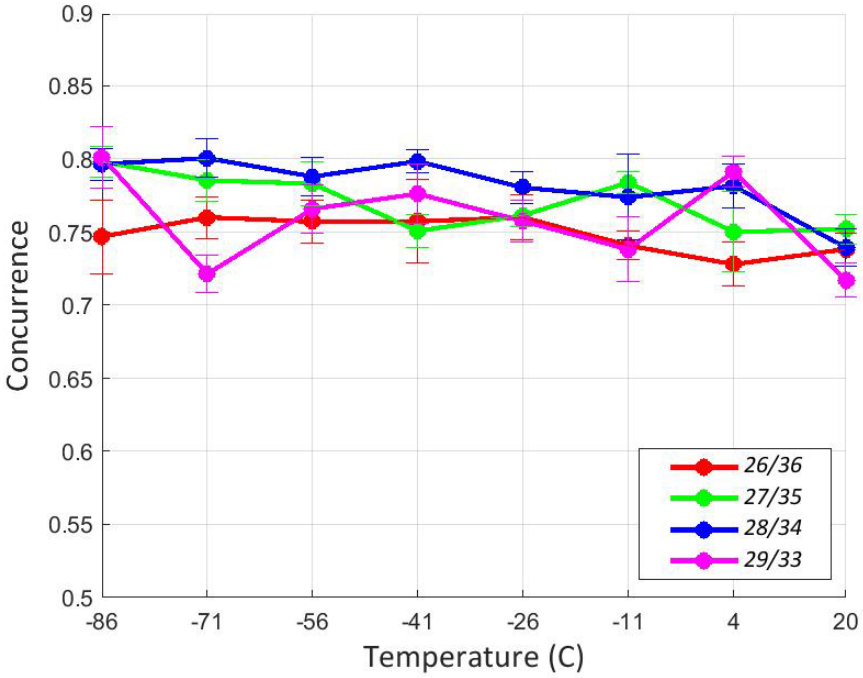


**Fig. 3 Concurrence as a function of temperature for the pump power that results in maximum concurrence (i.e., ~12.5 dB). The average concurrence for all channel pairs increases from 0.74 to 0.79 as the temperature of the DSF is decreased from +20 to –86 °C due to a reduction in Raman-scattered photons.**

## 3.2 Measure the Coincidence-to-Accidental Ratio

To perform CAR measurements, start by physically disconnecting the fibers from the PAs and connecting the EPS output channels directly to the CPDS. As described in Section 2.3, ensure that the appropriately correlated channel pairs are used when connecting the EPS to the CPDS. Prior to connection, make sure to follow the fiber cleaning procedures described earlier. Next, adjust the freezer temperature to the desired temperature. Here, the freezer was only set to two different temperatures: +20 and –86 °C.

For CAR measurements, we chose to not take measurements for channel pair 29/33 for two reasons. First, the concurrence values determined by tomography clearly showed that Channels 29/33 have the lowest entanglement quality. Therefore, further investigation of those channels was not necessary. Second, preliminary measurements of Channels 29/33 showed significantly increased singles count rates

in agreement with our hypothesis that the drastically reduced concurrence of photons in Channels 29/33 is due to the presence of SPM-broadened pump photons. Because of these very high count rates at the powers used in this report, we chose to not perform CAR measurements in Channels 29/33 to prevent damaging the SPDs in the CPDS.

Now open the EPA software on the laboratory computer. Follow the steps mentioned in Section 2.3 to identify all devices, initialize the EPS, scan the detector gate phase, and synchronize the detectors. Next, set the EPA light setting to the desired value. For the CAR measurements described here, we varied the light setting from 2800 to 3600. Once again, record the power displayed on the EPS for each light setting entered in the EPA software. We used a lower power range for the CAR measurements than for the tomography measurements in order to characterize the EPS over a wider range of input parameters. CAR measurements can be performed much faster than tomography since count rates are greater (because no PAs are used) and only one measurement is required (instead of 36). Performing tomography at powers as low as 2800 would have taken an impractically long amount of time to achieve a sufficient number of counts. For example, we used $10^9$ detection gates (20 min) per CAR measurement for the lowest power data points (i.e., for a light setting of 2800) to obtain a sufficiently high number of coincidences. To perform tomography with the same number of gates per measurement would take 12 h per individual tomography. Performing tomography 10 consecutive times per data point as we did here would have taken 5 days.

Next set the number of gates to the desired amount and press the "measure" button. Recall that the number of gates should be set to ensure that at least 1000 coincidences are detected. When clicking "measure," the CPDS measures the number of single counts for both detectors, coincidences, and accidental coincidences for the set number of gates, and the EPA software displays the results. All measurements must then be recorded manually, including the light setting, power on the EPS front panel, and measurement results (singles, coincidences, and accidental coincidences). Record the measurement results for each power setting and then repeat the process for all remaining correlated channel pairs at the same temperature. Finally, repeat all of the steps for each temperature.

The CAR is shown for each channel pair as a function of attenuation at +20 and –86 °C in Figs. 4(a) and (b), respectively. For both temperatures, the CAR is maximized for a pump attenuation of approximately 14 dB and then decreases as the power is increased. Similar to the tomography results described in Section 3.1, this indicates the presence of noise photons due to SPM-induced broadening of the pump. For both temperatures, Channels 28/34 achieve the highest CAR, followed by Channels 27/35 and then Channels 26/36. The maximum CAR for Channels

28/34 increases from 15.1 at 20 °C to 23.4 at –86 °C due to the decrease of Raman-scattered noise photons.

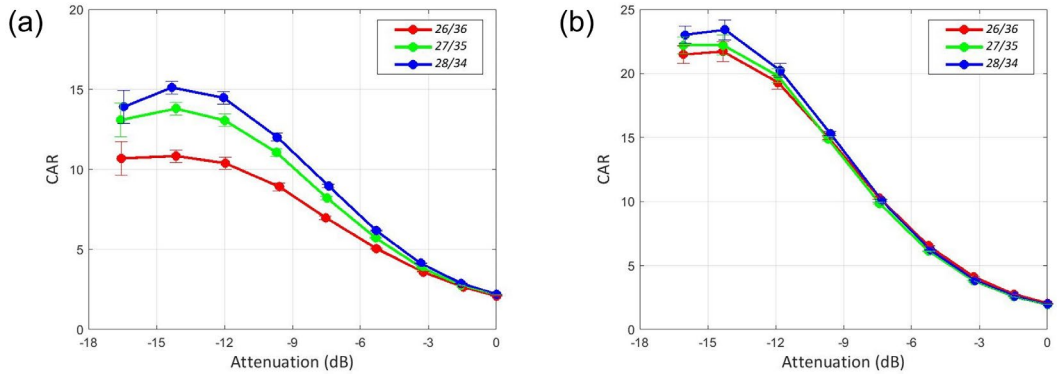


**Fig. 4 CAR as a function of pump attenuation when the DSF is stored at (a) +20 °C and (b) –86 °C. The CAR is greater when the DSF is stored at –86 °C due to a reduction in the amount of Raman-scattered noise photons. Error bars are calculated from the standard deviation of 10 consecutive measurements and are smaller than the point size in some cases due to the large number of counts per measurement.**

## 4. Conclusion

Quantum network users require intimate knowledge of their EPS performance, the types of noise photons that are output by the source, and the regimes that their sources must be operated in to maximize entanglement quality. In this report we described a method to characterize the behavior of the NuCrypt entangled photon distribution system as a function of temperature, power, and frequency. We analyzed the entangled source performance by performing quantum state tomography, by calculating the concurrence of the quantum state output by the EPS, and by measuring the CAR of light output by the EPS. We found that noise photons due to Raman-scattering and spectral broadening of the pump caused by SPM significantly reduce the performance of the source in certain operating regimes.

To reduce the amount of Raman-scattered noise photons and to therefore increase the entanglement quality of photons output by the source, we showed that the dispersion-shifted fiber in which the photons are generated should be cooled to the lowest temperature possible (–86 °C for the freezer used in our lab). The number of Raman-scattered photons could be further reduced by cooling the DSF to even lower temperatures, for example by submerging the DSF in liquid nitrogen as opposed to using a freezer. In addition, we showed that the pump power should also be reduced to minimize the relative amount of SPM photons output by the source, further increasing the entanglement quality. While lowering the pump power does indeed increase the entanglement quality, there is an inherent trade-off of a reduced transmission rate of entangled photon pairs for lower pump powers.

## 5. References


1. Fiorentino M, Voss PL, Sharping JE, Kumar P. All-fiber photon-pair source for quantum communications. IEEE Photon Technol Lett. 2002;14:983–985.

2. Inoue K. Four-wave mixing in an optical fiber in the zero-dispersion wavelength region. J Lightwave Technol. 1992;10:1553–1561.

3. NuCrypt, LLC. Product overview: quantum optical instrumentation; n.d. [accessed 2022 Sep]. http://www.nucrypt.net/quantum-optical -instrumentation.html.

4. Wang SX, Kanter GS. Robust multiwavelength all-fiber source of polarization-entangled photons with built-in analyzer alignment signal. IEEE J Sel Top Quantum Electron. 2009;15:1733–1740.

5. Jones DE, Weninger D, Brodsky M. Setting single photon detectors for use with an entangled photon distribution system. Army Research Laboratory (US); 2017. Report No.: ARL-TR-8229.

6. Ma X, Yang L, Guo X, Li X. Generation of photon pairs in dispersion shift fibers through spontaneous four wave mixing: influence of self-phase modulation. Opt Commun. 2011;284:4558–4562.

7. Morosova A, Jones DE, Brodsky M. Noise photons due to self-phase modulation in an entangled photon source. CCDC Army Research Laboratory (US); 2019 Sep. Report No.: ARL-TR-8790.

8. Stolen RH, Ippen EP, Tynes AR. Raman oscillation in glass optical waveguide. Appl Phys Lett. 1972;20:62–64.

9. Newbury NR. Pump-wavelength dependence of Raman gain in single-mode optical fibers. J Lightwave Technol. 2003;21:3364.

10. Voss PL, Kumar P. Raman-noise-induced noise-figure limit for $\chi(3)$ parametric amplifiers. Opt Lett. 2004;29:445–447.

11. Voss PL, Kumar P. Raman-effect induced noise limits on (3) parametric amplifiers and wavelength converters. J Opt B Quantum Semiclassical Opt. 2004;6:S762.

12. Jones DE, Kirby BT, Brodsky M. Tuning quantum channels to maximize polarization entanglement for telecom photon pairs. NPJ Quantum Inf. 2018;4:58.

13. Kirby BT, Jones DE, Brodsky M. Effect of polarization dependent loss on the quality of transmitted polarization entanglement. J Light Technol. 2019;37:95–102.

14. Jones DE, Kirby BT, Riccardi G, Antonelli C, Brodsky M. Exploring classical correlations in noise to recover quantum information using local filtering. New J Phys. 2020;22:073037.

15. Riccardi G, Antonelli C, Jones DE, Brodsky M. Simultaneous decoherence and mode filtering in quantum channels: theory and experiment. Phys Rev Appl. 2021;15:014060.

16. Riccardi G, Jones DE, Yu XD, Gühne O, Kirby BT. Exploring the relationship between the faithfulness and entanglement of two qubits. Phys Rev A. 2021;103:042417.

17. Inoue K, Shimizu K. Generation of quantum-correlated photon pairs in optical fiber: influence of spontaneous Raman scattering. Jpn J Appl Phys. 2004;43:8048.

18. Li X, Chen J, Voss PL, Sharping J, Kumar P. All-fiber photon-pair source for quantum communications: improved generation of correlated photons. Opt. Express. 2004;12:3737–3744.

19. Li X, Voss PL, Chen J, Lee KF, Kumar P. Measurement of co- and cross-polarized Raman spectra in silica fiber for small detunings. Opt Express. 2005;13:2236–2244.

20. Takesue H, Inoue K. 1.5-μm band quantum-correlated photon pair generation in dispersion-shifted fiber: suppression of noise photons by cooling fiber. Opt Express. 2005;13:7832–7839.

21. Lee KF, Chen J, Liang C, Li X, Voss PL, Kumar P. Generation of high-purity telecom-band entangled photon pairs in dispersion-shifted fiber. Opt Lett. 2006;31:1905–1907.

22. Lin Q, Yaman F, Agrawal GP. Photon-pair generation in optical fibers through four-wave mixing: role of Raman scattering and pump polarization. Phys Rev A. 2007;75:023,803.

23. Goldschmidt EA, Eisaman MD, Fan J, Polyakov SV, Migdall A. Spectrally bright and broad fiber-based heralded single-photon source. Phys Rev A. 2008;78:013,844.

24. Dyer SD, Stevens MJ, Baek B, Nam SW. High-efficiency, ultra-low-noise all-fiber photon-pair source. Opt Express. 2008;16:9966–9977.

25. Jones DE, Kirby BT, Brodsky M. Joint characterization of two single photon detectors with a fiber-based source of entangled photon pairs. Frontiers in Optics 2017. Optical Society of America Paper No.: JW4A.37. https://opg.optica.org/abstract.cfm?uri=fio-2017-JW4A.37.

26. Jones DE, Kirby BT, Brodsky M. In-situ calibration of fiber-optics entangled photon distribution system. In: Proceedings of the IEEE Photonics Society Summer Topical Meeting Series; 2017. p. 123–124.

27. Altepeter JB, Jeffrey ER, Kwiat PG. Photonic state tomography. In: Berman PR, Lin CC, editors. Advances in atomic, molecular, and optical physics. Elsevier; 2005. p. 105–159.

28. Smolin JA, Gambetta JM, Smith G. Efficient method for computing the maximum-likelihood quantum state from measurements with additive gaussian noise. Phys Rev Lett. 2012;108:070502.

29. Lohani S, Kirby BT, Brodsky M, Danaci O, Glasser RT. Machine learning assisted quantum state estimation. Mach Learn Sci Technol. 2020;1:035007.

30. Danaci O, Lohani S, Kirby BT, Glasser RT. Machine learning pipeline for quantum state estimation with incomplete measurements. Mach Learn Sci Technol. 2021;2:035014.

31. Lohani S, Lukens JM, Glasser RT, Searles TA, Kirby BT. Data-centric machine learning for quantum information science. Mach Learn Sci Technol. 2022;3:04LT01.

32. Lohani S, Searles TA, Kirby BT, Glasser RT. On the experimental feasibility of quantum state estimation via machine learning. IEEE Trans on Quant Eng. 2020;2:2103410.

33. Lukens JM, Law KJH, Jasra A, Lougovski P. A practical and efficient approach for Bayesian quantum state estimation. New J Phys. 2020;22:063038.

34. Lohani S, Lukens JM, Jones DE, Searles TA, Glasser RT, Kirby BT. Improving application performance with biased distributions of quantum states. Phys Rev Res. 2021;3:043145.

## List of Symbols, Abbreviations, and Acronyms

| | |
|---|---|
| ARL | Army Research Laboratory |
| CAR | coincidence to accidental ratio |
| CC | coincidence-counting electronics |
| CPDS | correlated photon detection system |
| DEVCOM | US Army Combat Capabilities Development Command |
| DSF | dispersion-shifted fiber |
| EPA | Entangled Photon Analyzer |
| EPS | entangled photon source |
| FWM | four-wave mixing |
| InGaAs | indium gallium arsenide |
| ITU | International Telecommunication Union |
| MLE | maximum likelihood estimation |
| PA | polarization analyzer |
| PBS | polarizing beam splitter |
| PC | polarization controller |
| SPD | single photon detector |
| SPM | self-phase modulation |
| USB | Universal Serial Bus |
| μW | microwatts |

| | |
|---|---|
| 1 (PDF) | DEFENSE TECHNICAL INFORMATION CTR DTIC OCA |
| 1 (PDF) | DEVCOM ARL FCDD RLD DCI TECH LIB |
| 2 (PDF) | DEVCOM ARL FCDD RLC NT D JONES B KIRBY |